SEYBOLD Report
ISSN: 1533 - 9211
https://seyboldreport.net/

HYDROTHERMAL PRODUCTION, CHARACTERIZATION, ANTIBACTERIAL ACTIVITY AND HUMIDITY SENSOR APPLICATION OF CERIUM OXIDE NANOPARTICLES

Dr. Manda Saritha
St. Peter's Engineering College, Hyderabad
Email: mandasaritha04@gmail.com

Mr. Gaurav singh
St. Peter's Engineering College, Hyderabad
Email: gauravnanotechnology@gmail.com

Dr Asif Jamal G.A
Department of Botany, Justice Basheer Ahmed Sayeed College for Women (Autonomous)
Chennai, Tamil Nadu, Email: drasifjamal1978@gmail.com

Dr. Prasanna Srinivas R
Department of Microbiology, M.S Ramaiah College of Arts, Science and Commerce
Bengaluru, Karnataka, Email: microprasanna@gmail.com

Dr. Vinayaka K. S
Department of Botany, Sri Venkataramana Swamy College, Vidyagiri, Bantwal, Karnataka
Email: ks.vinayaka@gmail.com

Dr. Suman Pawar
Dept of Chemical Engineering, Siddaganga Institute of Technology, Tumkur
Email: svp@sit.ac.in

ABSTRACT

Using a hydrothermal technique and various surfactants, including polyethylene glycol (PEG), cetyltrimethylammonium bromide (CTAB), and sodium dodecyl benzenesulfonate (SDBS), nanosized CeO_2 powders were created. Transmission electron microscopy, Raman spectroscopy, and X-ray diffraction were all used to analyse the products' phase structures and morphologies. Between these three samples, the one containing CTAB as the surfactant (CeO_2-C) has the highest specific surface area and the lowest particle size. In comparison to those made using CeO_2-P and CeO_2-S, the humidity sensor created with CeO_2-C performs better. With a change in relative humidity (RH) from 15.7 to 95%, the CeO_2-C sensor's impedance falls by nearly five orders of magnitude. The response and recovery times are, respectively, 7 and 7 s. These findings suggest that the addition of cationic surfactant can significantly enhance the performance of CeO_2 humidity sensors. The antibacterial activity was performed against a set of bacterial strains shows CeO_2 NPs possessed significant antibacterial properties

Keywords: CeO_2 nanopowders, humidity sensor, hydrothermal, Cerium nano particles and

antibacterial activity.

1. INITIALIZATION

Since vapour concentration has been recognised as being crucial to industrial output, agriculture, and environmental protection, humidity sensors have attracted a lot of attention [1-4]. Organic polymer films and porous ceramic films are typically used as humidity sensor materials [5, 6]. The main drawbacks of humidity sensors based on the first are their low operating temperature, insufficient mechanical strength, and poor physical and chemical stability. The biggest difficulty for the latter is the slow response and recovery time. Numerous initiatives have been made in recent years to investigate the materials used in humidity sensors, including SnO_2, TiO_2, ZnO, and $BaTiO_3$ [7–10]. Cerium oxide, one of the potential materials for sensors, exhibits a high oxygen vacancy diffusion coefficient as well as good corrosion resistance to corrosive gases (Cl_2, SO_2, and NO) [11].Based on the previously noted merit, CeO_2 has recently generated a lot of discussion.

Several strategies have been put forth in the last few years to create fine nanopowders. Due to the benefits of homogenous nucleation processes and tiny particle size, the hydrothermal approach is seen to be one of the most promising technologies for producing nanopowders at room temperature. However, nanoparticles are easily coagulated and hard to disperse due to the high surface energy. It is widely known that severe agglomeration during the filming process has a negative impact on the properties of sensors. Different surfactant types have been developed to enhance the functionality of the materials [12, 13]. To the best of our knowledge, however, no systematic study of the impact of several surfactant types (nonionic, cationic, and anionic) on the functionality of CeO_2 as a humidity sensor has been published. Understanding the characteristics of various surfactants is crucial for enhancing the performance of sensing materials.

In this study, CeO_2 nanopowders were made using a hydrothermal process and three different types of surfactants—PEG (nonionic), CTAB (cationic), and SDBS (anionic)—were used as surfactants. The effects of these surfactants on the structures and humidity sensing capabilities of the corresponding sensors were thoroughly examined. This study's primary goal is to elucidate how surfactants affect the effectiveness of the CeO_2 humidity sensor.

2. EXPERIMENTATION SPECIFICS

The following steps were used to create CeO_2 nanopowders using various surfactants based on the traditional hydrothermal method: The starting material and surfactants utilised were $Ce(NO_3)_3$ $6H_2O$ (99.99%, Chenghai Chemical of Guangdong), CTAB, PEG, and SDBS (Shanghai Chemicals Ltd.). Under magnetic stirring, a specific quantity of surfactants (2 wt%) was added to 50mL of $Ce(NO_3)_3$ solution (0.1 M). Sodium hydroxide solution was added to the solution to bring the pH level down to 7. (2M). The mixed solution was then hydrothermally treated at 180°C for 24 hours in a Teflon autoclave to produce CeO_2 nanopowders. The precipitates were filtered, repeatedly rinsed with distilled water and ethanol, then dried for 12 hours at 70°C. The same process was used to create CeO_2 nano crystalline powders utilising CTAB, PEG, and SDBS as the appropriate surfactants. Three CeO_2 nanopowders were created and are referred to in this study as CeO_2-P, CeO_2-C, and CeO_2-S, respectively.

Using a Bruker D8 Focus powder X-ray diffractometer with Cu K radiation (=1.5406 A) with a scanning rate of 5 min1, the crystalline phases of CeO_2 nano crystalline powders were studied. The operating current was kept at 40 mA, and the voltage was kept at 40 kV. Based on these XRD patterns, the lattice parameters were computed. Using Scherrer's equation [14], it was possible to determine the average particle size of nanopowders (D):

$$D = \lambda \frac{K}{\beta \cos\theta}, \quad (1)$$

Where K is a constant (0.89), is the corrected full-width half maximum, is the diffraction angle, and is the X-ray radiation's wavelength (FWHM). For the instrument correction, the Gaussian-Gaussian relationship [14] was also used

$$\beta^2 = B^2 - b^2, \quad (2)$$

Where B and b, respectively, stand for the sample's FWHM and the reference silicon sample's standard width On a Thermo Nicolet 960 instrument, FT-Raman spectra were captured with an excitation wavelength of 1064 nm, and the measured wave number range is between 100 and 900 cm1. By using Micromeritics ASAP 2020 equipment and the Brunauer-Emmet-Teller (BET) equation, the specific surface area (SBET) was calculated. A Philips TF-F20 electron transmission microscope was used to look at the three samples' microstructures, morphologies, and particle sizes.

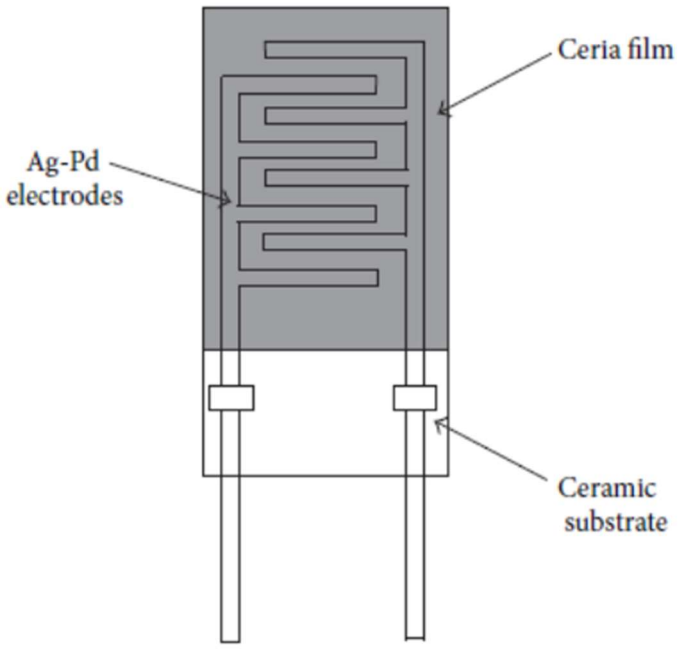

Figure – 1: Sensor structure

The CeO_2 nanopowders were distributed in ethanol by magnetic stirring to create the humidity sensors (30min). Using two Ag-Pd interdigital electrodes, the combined solution was dropped onto a ceramic substrate measuring 6 cm by 3 cm and 0.5 cm thick to create a 10 m-thick CeO_2 film. The humidity sensors were also annealed for 1 hour at 180 C. On a ZL-5 type LCR analyzer the characteristic curves of humidity sensitivity were measured (Shanghai,

China). The voltage in our investigation was set at 1V. The saturated salt solutions of $MgCl_2$, Mg(NO3)3, NaCl, KCl, and KNO_3 were used to create the humidity conditions, and the corresponding RH values were 33, 54, 75, 85, and 95%, respectively. An automatic dryer maintained a 15.7% RH humidity level in the lab environment. Figure 1 depicts the sensor structure's schematic diagram.

3. ANTIBACTERIAL ASSAY

Antibacterial activity of the CeO_2 NPs were carried out by the well method against the bacterial strains of (K. pneumonia (1), S. aureus (2), S. dysenteriae (3), E. coli (4), P. aeruginosa (5), S. pneumonia (6) and P. vulgaris (7)) on Mueller hinton agar, according to the Clinical and Laboratory Standards Institute (CLSI). Media plate's Mueller hinton agar (MHA) was streaked with bacteria 2-3 times by rotating the plate at 60° angles for each streak to ensure the homogeneous distribution of the inoculums. inoculation, discs (6 mm Hi-Media) loaded 1.5 mg/ml and 1.75 mg/ml, of the test samples were placed on the bacteria-seeded well plates using micropipettes. Plates were then incubated at 37°C for 24 h. inhibition zone around the well was measured and recorded. Amoxicillin (Hi-Media) was used as the positive controls against (K. pneumonia (1), S. aureus (2), S. dysenteriae (3), E. coli (4), P. aeruginosa (5), S. pneumonia (6) and P. vulgaris (7)) bacteria respectively. positive controls results were as compared to that of the of the test CeO_2 samples.

4. FINDINGS AND ANALYSIS

Figure 2 displays the findings of the XRD analysis of the crystal structures of the products as-prepared (a). Three samples' XRD patterns reveal ceria's [JCPDS 43-1002] face-centered cubic structure. According to Figure 2(a), the (111), (200), (220), (311), and (400) reflections are responsible for the peaks at round 2 = 29.8, 34.6, 49.6, 59.2, and 72.8, respectively. It is important to note that CeO_2-C has the smallest grain size among the three samples based on the fact that its diffraction peak width is wider than that of CeO_2-P and

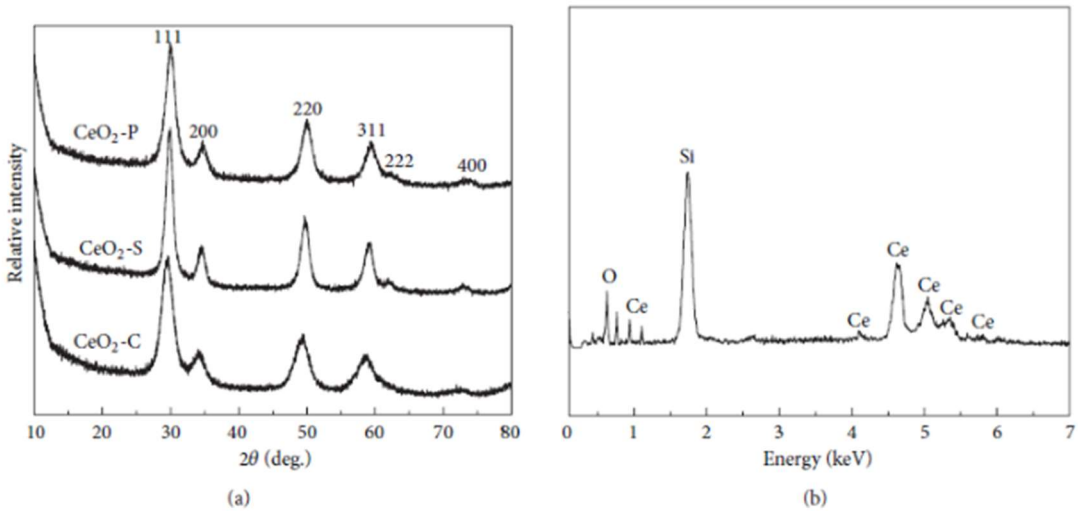

Figure – 2(a) and (b): XRD analysis of the crystal structures

CeO_2-S.An energy dispersive X-ray spectrometer was also used to further investigate

the composition of the as-produced goods (EDS). Only three elements (Ce, O, and Si) can be seen in the EDS spectrum of CeO_2-C, which is depicted in Figure 2(b). CeO_2-C's chemical make-up is very similar to CeO_2's stoichiometric make-up. The Si substrate is likely to blame for the presence of Si in the spectrum. In addition, three samples' average crystallite diameters, specific surface areas, and lattice characteristics were examined, as indicated in Table 1. Scherrer's equation was used to determine the crystal size, as described in the experimental part. Average crystallite sizes for CeO_2-C are 17.34 nm, 19.27 nm, and 21.42 nm for CeO_2-P and CeO_2-S, respectively. Using the software JADE 5.0, the lattice parameters are estimated from the XRD patterns. The determined value of each lattice parameter is the average value of 5 samples. Compared to CeO_2-P (5.3726 0.0002 nm) and CeO_2-S (5.3544 0.0003 nm), CeO_2-C has a computed value of 5.3945 0.0002 nm, which is greater. The values for CeO_2-C, CeO_2-P, and CeO_2-S in terms of specific surface area are 143.45, 116.87, and 99.36m2 g1, respectively. The specific surface area and crystal size for nanomaterials are tightly correlated. The particular surface area increases with decreasing crystal size. The specific surface areas of these three samples should decline in the following order: CeO_2-C > CeO_2-P > CeO_2-S, according to the statistics on average particle sizes indicated above. This trend and the measurement data used in this investigation are congruent. It is common knowledge that various optional adsorption mechanisms and interactions between the surfactant and inorganic precursor molecules during the nucleation process can have an impact on the structure, surface area, and crystallite size. The associated mechanism, however, is more intricate and requires additional research.

Table 1: The specific surface areas, crystalline sizes, and lattice parameters for three samples.

Samples	Specific surface area ($m^2 \cdot g^{-1}$)	Crystallite size (nm)	Lattice parameter (nm)
CeO_2-P	116.87	19.27	5.3726 ± 0.0002
CeO_2-C	143.45	17.34	5.3945 ± 0.0002
CeO_2-S	99.36	21.42	5.3544 ± 0.0003

Table – 1: The specific surface areas, crystalline sizes, and lattice parameters for three samples.

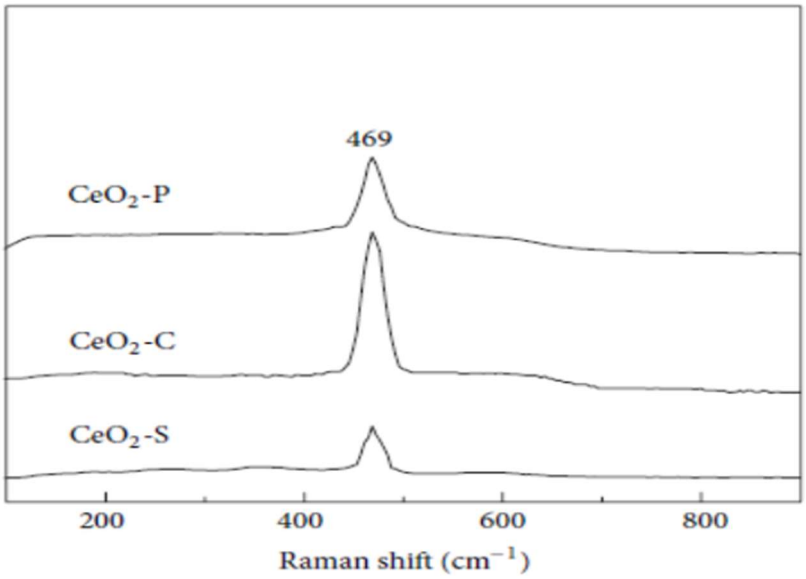

Figure – 3: Raman spectroscopy phase structure

The as-prepared samples were subsequently analysed by Raman spectroscopy in the wave number range of 100900 cm1 to confirm the phase structure, as shown in Figure 3. An intricate cubic type structure was discovered after careful analysis of the spectra. Figure 3 shows that the F2g vibration mode from the space group Fm3m of cubic structure is responsible for the major band at 469 cm1 [17, 18]. This further demonstrates that the three samples' structures are cubic phase, as indicated by the XRD study. Additionally, a little shoulder that should be identified as the longitudinal optical mode appeared at a distance of around 600 cm1 may be seen [19]. In this instance, CeO_2-C has a band at 469 cm1 with a higher intensity than the other two samples.

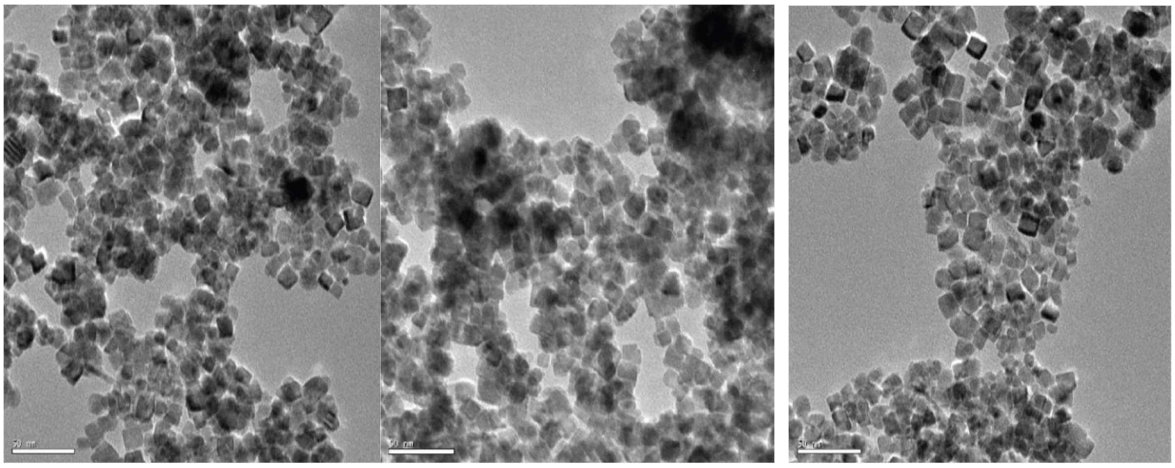

Figure - 4 Morphologies and particle sizes by TEM

Three samples' morphologies and particle sizes were examined by TEM, as illustrated in Figure 4. These three samples all exhibit a mono dispersed square shape, with CeO_2-C particles having more uniform sizes than CeO_2-P and CeO_2-S. The determined particle size was the average value of the 40 randomly chosen particles in the figure. The average particle sizes of three samples were also calculated. The calculated average particle sizes for CeO_2-P, CeO_2-C, and CeO_2-S are 19.76, 17.88, and 21.77 nm, respectively. These outcomes are in line with

earlier XRD analysis data that was previously mentioned. Figure 5 displays the resistance (R) vs. relative humidity (RH) characteristics of three samples using various surfactants, determined at room temperature, in the relative humidity range of 15.7% to 95%. Surfactants clearly have a significant impact on this study's findings about how humidity affects the impedance of sensors. Comparing these three samples, CeO_2-C exhibits a higher drop in impedance than CeO_2-P and CeO_2-S. CeO_2-C had the highest humidity sensitivity and the best linearity of the impedance versus RH curve. The scenario is exactly the opposite compared to CeO_2-C in the case of CeO_2- S. Furthermore, the impedance change for CeO_2-C exceeds five orders of magnitude.

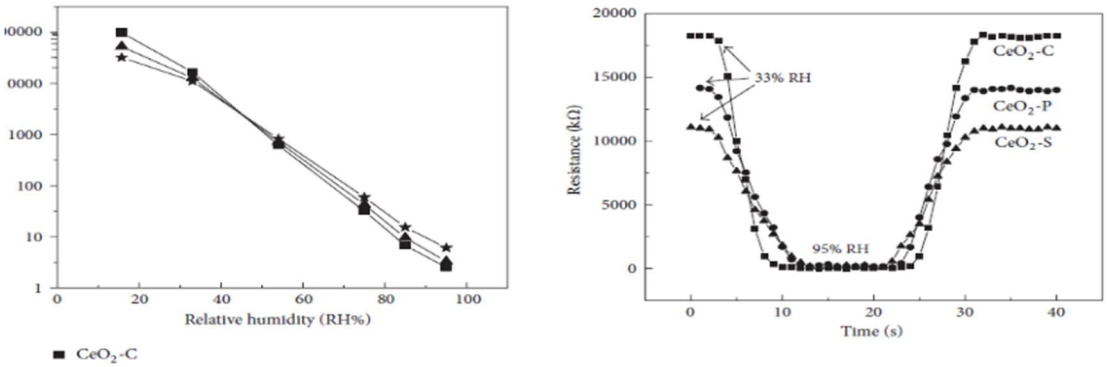

Figure – 5 and 6: Resistance (R) vs. relative humidity (RH) and the CeO_2-C humidity sensor of sample.

The important behaviours for measuring the performance of a humidity sensor are response and recovery behaviours. The amount of time it takes the sensor to acquire a 90% variable quantity is referred to as the response time for the adsorption process and the recovery time in the case of desorption. The reaction and recovery behaviours of three samples were examined in light of the aforementioned results. To evaluate the response and recovery time, the sensor is transferred from the initial atmosphere (33% RH) to the target atmosphere (95% RH), then transferred back. The CeO_2-C humidity sensor, as depicted in Figure 6, exhibits quick reaction and recovery properties. Response (humidification from 33 to 95% RH) and recovery (desiccation from 95 to 33% RH) times are each approximately 7 seconds long. However, the comparable response and recovery times for CeO_2-P and CeO_2-S are 10, 9 s and 12, 11 s, respectively. These results show that the cationic surfactant (CTAB) significantly enhances the functionality of CeO_2 humidity sensors.

It is generally known that the process by which water molecules adhere to the surface of nanoparticles plays a key role in humidity sensing. The amount of water molecules that are adsorbed on the powders has a significant impact on how the electrical response behaves. Only a small number of water molecules can be adsorbed on the surface of the film by the chemisorption mechanism under conditions of low humidity [20–22]. The difficulty of electrolytic conduction is caused by the layer of water molecules that is not continuous on the surface of the film. Studies by Schaub et al. [23–25] indicate that the high local charge density and strong electrostatic field caused by the powders' flaws, tips, and contractions can encourage water dissociation to produce charge carriers. However, with high humidity, physisorption

mechanisms can cause an increasing number of water layers to develop on nanoparticle surfaces. H+ formed from water molecules, which are the predominant charged carriers, might further reduce the impedance. However, in our investigation, the high specific surface area and nanosized grains also have a significant impact on the sensor performance.

Since there are so many more grain boundaries at the nanoscale, there are many more active locations for water molecule reactions. Additionally, of the three samples, the CeO_2-C nanoparticles have the highest specific surface area. Water molecules are readily absorbed on the surface of the sensor due to the large surface area of the nanomaterials, which can enhance response and recovery properties. As a result, CeO_2-C responds and recovers more quickly than CeO_2-P and CeO_2-S. According to the study's findings, it can be concluded that, when compared to nonionic surfactant (PEG) and anionic surfactant, cationic surfactant (CTAB) significantly improves the sensibility of CeO_2 humidity sensor (SDBS).

The size of the zone of inhibition and antibacterial activity formed around each well concentration (1.5 mg/ml and 1.75 mg/ml) of CeO_2 NPs loaded with test samples is depicted in Figures 7 and 8, which also show how CeO_2 NPs were tested against Gram-positive bacteria (S. aureus and S. pneumoniae) and Gram-negative bacteria (E. coli, P. aeruginosa, P. vulgaris, K. pneumonia, and S. dys.

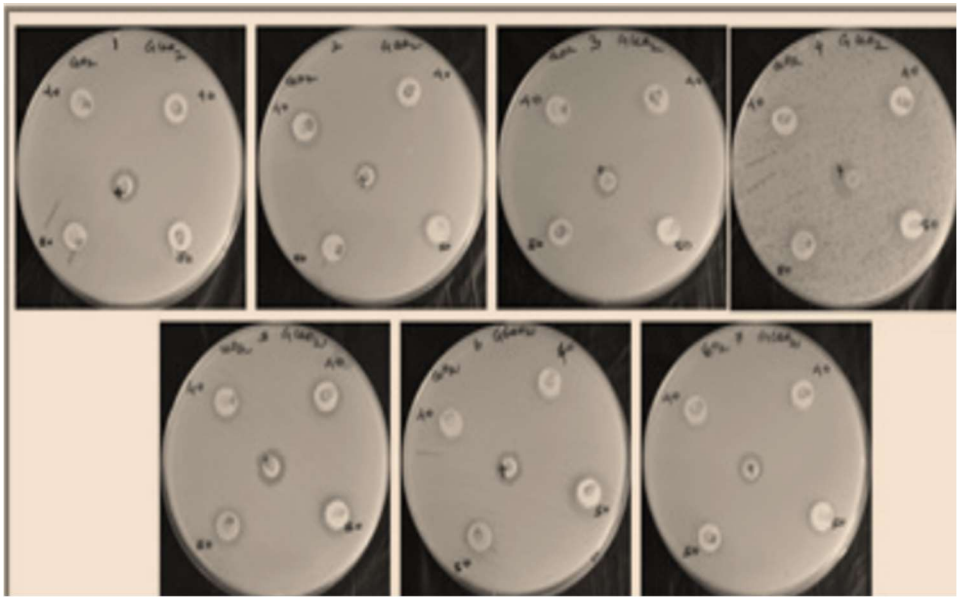

Figure 7: Antibacterial activity of the C-CeO_2

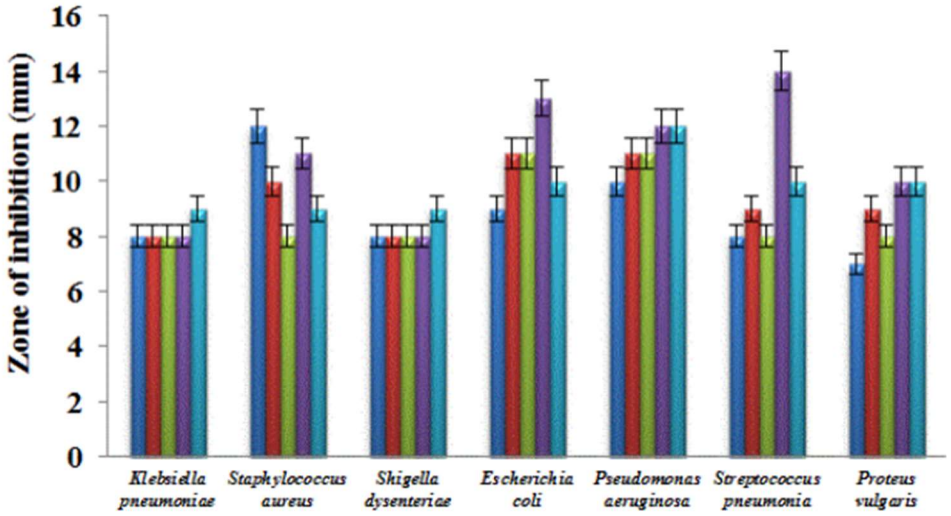

Figure 8: Zone of inhibition and antibacterial activity

NPs' antibacterial activity can either interact with microbial cells directly or result in secondary metabolites that harm the environment. are responsible for a number of the metal oxide nanomaterials' antibacterial properties.

4. CONCLUSION

CeO_2 nanoparticles with three different kinds of surfactants were produced by a hydrothermal method. CeO_2-C is the best in terms of both specific surface area and particle size. The performances of the relevant sensors were also thoroughly studied. Cationic surfactant (CTAB), as compared to anionic (SDBS) and nonionic (PEG), considerably enhances the performance of the humidity sensor. The CeO_2-C humidity sensor has high sensitivity, rapid response (7 s), and rapid recovery (7 s) characteristics in the humidity range of 33-95% RH, whereas the response and recovery periods for CeO_2-P and CeO_2-S are 10, 9 s and 12, 11 s, respectively. Studies showing CeO_2 NPs to have considerable antibacterial activity were conducted against a variety of bacterial species. According to the X-ray diffractogram,CeO_2 nanoparticles (NPs), which are smaller in size and have a wide interfacial area, are more effective against bacteria.

REFERENCES

[1] S. Zampolli, I. Elmi, J. St¨urmann, S. Nicoletti, L. Dori, and G. C.Cardinali, “Selectivity enhancement of metal oxide gas sensorsusing a micromachined gas chromatographic column,” Sensorsand Actuators B, vol. 105, no. 2, pp. 400–406, 2005.

[2] S. Ehrmann, J. J¨ungst, J. Goschnick, and D. Everhard, “Application of a gas sensormicroarray to human breath analysis,”Sensors and Actuators B, vol. 65, no. 1, pp. 247–249, 2000

[3] S. Yin, G.Wang, and H. Karimi, “Data-driven design of robust fault detection system for wind turbines,,” Mechatronics, 2013.

[4] S. Yin, H. Luo, and S.Ding, “Real-time implementation of faulttolerant control systems with performance optimization,” IEEE Transactions on Industrial Electronics, vol. 61, no. 5, pp. 2402–2411, 2014.

[5] X. Q. Fu, C. Wang, H. C. Yu, Y. G. Wang, and T. H. Wang, "Fast humidity sensors based on CeO2 nanowires," Nanotechnology, vol. 18, no. 14, Article ID 145503, 2007.
[6] S. Yin, S. Ding, A. Haghani, H. Hao, and P. Zhang, "A comparison study of bacis data-driven fault diagnosis and process monitoring methods on the benchmark Tennessee Eastman process," Journal of Process Control, vol. 22, no. 9, pp. 1567–1581, 2012.
[7] Q. Kuang, C. Lao, Z. L. Wang, Z. Xie, and L. Zheng, "High sensitivity humidity sensor based on a single SnO2 nanowire," Journal of the American Chemical Society, vol. 129, no. 19, pp. 6070–6071, 2007.
[8] G.Garcia-Belmonte,V. Kytin,T.Dittrlch, andJ.Bisquert, "Effect of humidity on the ac conductivity of nanoporousTiO2," Journal of Applied Physics, vol. 94, no. 8, pp. 5261–5264, 2003.
[9] Y. Qiu and S. Yang, "ZnO nanotetrapods: controlled vaporphase synthesis and application for humidity sensing," Advanced Functional Materials, vol. 17, no. 8, pp. 1345–1352,2007.
[10] J. Wang and G. Song, "Mechanism analysis of BaTiO3 and polymerQARcomposite humidity sensor," Thin Solid Films, vol 515, no. 24, pp. 8776–8779, 2007.
[11] E. B. V´arhegyi, I. V. Perczel, J. Gerblinger, M. Fleischer, H. Meixner, and J.Giber, "Auger and SIMS study of segregation and corrosion behaviour of some semiconducting oxide gas-sensor materials," Sensors and Actuators B, vol. 19, no. 1–3, pp. 569–572, 1994.
[12] R. R. Piticescu, C. Monty, D. Taloi, A. Motoc, and S. Axinte, "Hydrothermal synthesis of zirconia nanomaterials," Journal of the European Ceramic Society, vol. 21, no. 10-11, pp. 2057–2060, 2001.
[13] D. K. Smith and B. A. Korgel, "The importance of the CTAB surfactant on the colloidal seed-mediated synthesis of gold nanorods," Langmuir, vol. 24, no. 3, pp. 644–649, 2008.
[14] H. Y. Jin, N.Wang, L. Xu, and S. Hou, "Synthesis and conductivity of cerium oxide nanoparticles," Materials Letters, vol. 64, no. 11, pp. 1254–1256, 2010.
[15] S. Yin, S. Ding, A.Haghani, and H.Hao, "Data-driven monitoring for stochastic systems and its application on batch process," International Journal of Systems Science, vol. 44, no. 7, pp. 1366–1376, 2013.
[16] S. Brunauer, P. H. Emmett, and E. Teller, "Adsorption of gases in multimolecular layers," Journal of the American Chemical Society, vol. 60, no. 2, pp. 309–319, 1938.
[17] Z.D.Dohcevic-Mitrovic, M. J.˘S´cepanovi´c, M.U.Gruji´c-Broj˘cin et al., "The size and strain effects on the Raman spectra of Ce1-xNdxO2-δ ($0 < x < 0.25$) nanopowders," Solid State Communications, vol. 137, no. 7, pp. 387–390, 2006.
[18] S. Patil, S. Seal, Y. Guo, A. Schulte, and J. Norwood, "Role of trivalent La and Nd dopants in lattice distortion and oxygen vacancy generation in cerium oxide nanoparticles," Applied Physics Letters, vol. 88, no. 24, Article ID 243110, 2006.
[19] Z. Xu, S. He, L.He, R. Mu,G.Huang, and X. Cao, "Novel thermal barrier coatings based on La2(Zr0.7Ce0.3)2O7/8YSZ doubleceramic-layer systems deposited by electron beam physical vapor deposition," Journal of Alloys and Compounds, vol. 509, no. 11, pp. 4273–4283, 2011.
[20] X. Zhao, X. Liu, S. Yin, and H. Li, "Improved results on stability of continuous-time

switched positive linear systems," Automatica, 2013.
[21] W. M. Qu and W. Wlodarski, "A thin-film sensing element for ozone, humidity and temperature," Sensors and Actuators B, vol. 64, no. 1–3, pp. 42–48, 2000.
[22] X. Zhao, L. Zhang, P. Shi, and H. Karimi, "Robust control of continuous-time systems with state-dependent uncertainties and its application to electronic circuits," IEEE Transactions on Industrial Electronics, 2013.
[23] R. Schaub, P. Thostrup, N. Lopez et al., "Oxygen vacancies as active sites for water dissociation on rutile TiO2 (110)," Physical Review Letters, vol. 87, no. 26,Article ID 266104, 4 pages, 2001.
[24] X. Zhao, L. Zhang, P. Shi, and M. Liu, "Stability of switched positive linear systems with average dwell time switching," Automatica, vol. 48, no. 6, pp. 1132–1137, 2012.
[25] X.Zhao, L. Zhang, P. Shi, andM.Liu, "Stability and stabilization of switched linear systems with mode-dependent average dwell time," IEEE Transactions on Automatic Control, vol. 57, no. 7, pp.1809–1815, 2012.

,